XX IMEKO World Congress
Metrology for Green Growth
September 9–14, 2012, Busan, Republic of Korea

THE STRUCTURE OF FLOW FIELD IN SMALL SIZE VORTEX FLOW METERS

G. Loriel, and L. Nang Wei
ICAM, France
E. von Lavante, and A. Gedikli
University of Duisburg-Essen, Germany, Lotharstr. 1, D-43053 Duisburg
H. Krisch and S. Tournillon
Krohne Messtechnik GmbH, Germany

Abstract: In the present investigation, the problem of accurate determination of volumetric flows by means of vortex-shedding flow meters in the case of upstream disturbances produced by bends has been studied. To this end, the corresponding flow field was investigated experimentally and by detailed numerical simulation for the case of incompressible fluid flow (water). The computations were carried out for a limited number of cases using the three-dimensional unsteady incompressible solver of the Navier-Stokes equations as included in the adapco Star CCM+ commercial program.. The effects of turbulence were modelled using the realizable k-ε turbulence model. The resulting flow fields were studied in detail using various visualization methods. The effect of the disturbances was investigated for 3 different orientations of the basic meter relative to the bend. The effect of each of the cases was assessed by comparison with the undisturbed inflow into the meter. The resulting knowledge of the flow field in a vortex flow meter is highly useful not only for the understanding of the meters response to upstream disturbances, but it also offers a valuable tool for future developments.

Keywords: Vortex Flow Meters, Flow Simulation, Experimental Flow Metering, Accuracy, Upstream Disturbances.

1. INTRODUCTION

Many chemical and environmental processes found in the corresponding industries require volume- or mass flow data. One relatively simple flow measurement device applicable here is the so-called vortex-shedding flow meter (VFM), in which the volumetric flow is determined by observing the relationship between the vortex-shedding frequency from a bluff body attached inside a channel, and the corresponding mean velocity about it. The bluff body causes production of a system of periodic vortices (von Karman vortex street), whose frequency can be correlated with the mean flow velocity and, therefore, the volumetric flow. This procedure assumes a regular and well defined vortex structure as well as shedding mechanism, requiring linear dependency of the volumetric flow on the shedding frequency over a wide range of Reynolds numbers. In Fig. 1, the numerically simulated flow field about a typical VFM as produced by Krohne Messtechnik GmbH is displayed.

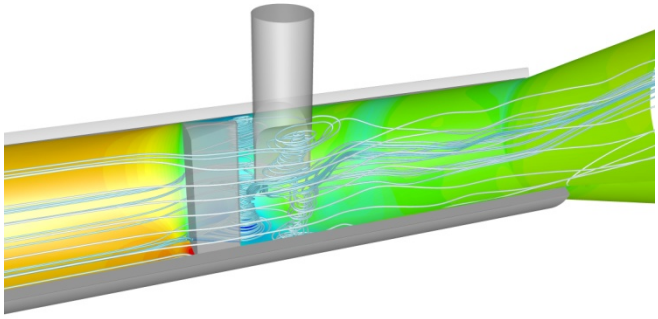

Figure 1: Flow field in a typical VFM

Downstream of the bluff body of width D (diameter of the test section), von Karman vortex street develops; the vortex shedding frequency f and the distance T between the vortices depend on the bluff body's shape, the bulk velocity, and the fluid properties. It can be easily shown by dimensional analysis that the Strouhal number Sr:

$$Sr = (D \cdot f) / u_m$$

has to depend uniquely on the pipe flow Reynolds number, assuming incompressible flow with maximum Mach number below 0.3. Many times, however, the frequency is expressed as the dimensional k-factor:

$$k = f / Q$$

with Q being the volumetric flow.

Commercial vortex flow meters use a large variety of bluff body shapes, test sections (conical inflow and outflow, constrictors of various shapes) and signal detection systems (pick-up). The corresponding flow fields have been studied by, among others, von Lavante et al. [1] using a combination of numerical simulations and global experiments for validation. The signal detection and processing have been discussed by Hans et. al. [3] and [4]. It has been also observed that a slight uncontrolled modification of the assumed geometry of a particular vortex-shedding flow meter, e.g. shape, location relative to the surrounding casing

and change of shape due to wear caused by particles suspended in the metered fluid, could cause a shift of its characteristic frequencies, leading to unreliable volumetric flow data. The influence of the manufacturing tolerances on the accuracy of vortex-shedding flow meters and abrasion by particles suspended in the metered fluid has been investigated in [5] and [6] by von Lavante et al. A detailed study of the flow field in small size commercial vortex-shedding flow meters with inflow and outflow conditioned by a Venturi nozzle and a diffusor has been published by von Lavante et al. in [2].

In the present investigation, a typical Krohne Messtechnik VFM DN 25 has been investigated using water as the metered fluid. For the time being, the upstream disturbance was generated by a single bend oriented as shown in Fig. 2. The flow field was studied for 3 different relative positions between the bend plane and the paddle of the VFM, as given in Fig. 3. The water was entering the bend at a bulk velocity of 2 m/s. The undisturbed flow field was studied in detail before being compared with the disturbed flow in the meter. Conclusions about the influence of the different types of disturbances were drawn.

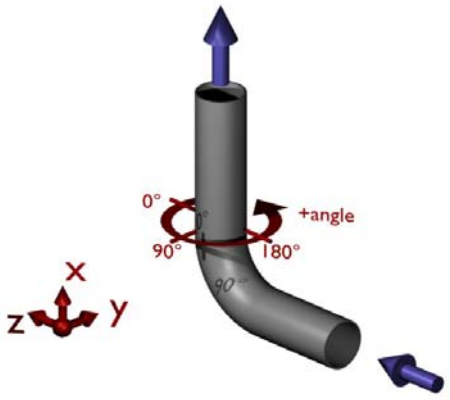

Figure 2: Definition of the coordinate system

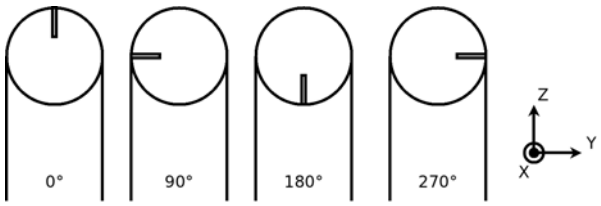

Figure 3: Relative position between the bend and the pickup sensor (paddle) of the VFM: 0°, 180° and 90°

2. DISCRIPTION OF THE CASES STUDIED

In the present work, in was decided to concentrate first on the single bend at 90° angle at different orientations relative to the meter. The bend confirmed to the OIML standard, having a radius of curvature R = 1.5 D. The experimental work was performed for different bulk velocities (Reynolds numbers) and distances between the VFM, defined by the location of the bluff body (BB), and the outlet from the bend. The vortex frequencies were detected by means of a paddle protruding from one side of the metering section, as shown in Fig. 1. It exerted a significant influence on the flow field, which will be discussed later.

The numerical simulations were carried out using the commercial program StarCCM+ on structured grids generated by a program called Gridgen. Due to the high resolution of the grids and complexity of the configuration, excessive computational times in order of weeks were the rule. Therefore, in most of the realistic simulations that included the bend and the VFM, only one velocity, typical for the operation of the meter, was selected, resulting in a bulk velocity of 2 m/s. The resulting flow field just after the bend (well known, but displayed here as a reminder) can be seen in Figure 4 below.

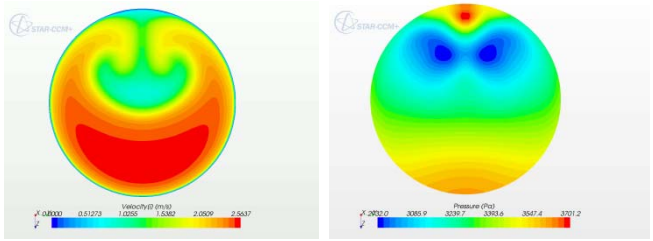

Figure 4: Left, axial velocity distribution; right, static pressure after a single bend

In Fig. 4, the positive z-axis is showing down in vertical direction, so that the bend is oriented upward. The flow is observed looking in the positive x-direction, i.e. downstream. Clearly visible is the non-uniform distribution of the axial velocity. The two secondary vortices can be seen in the right picture as locations of static pressure minimum. Although they seem to be symmetric about the z-x plane, this symmetry was obtained only after averaging the resulting flow field over a long time period. The two vortices are unsteady, alternating their strength periodically. Consequently, the simulations had to be carried out in unsteady mode.

In the previous descriptions of the flow field, one would mostly see the flow features displayed on the axial plane, showing the vortex street. This picture is, however nice and understandable, oversimplified, as highly three dimensional structures will be found in the wake of the BB. Nonetheless, for better understanding of the following discussion, the same axial plane display is given in Figure 5 for undisturbed flow of water at 2 m/s bulk velocity.

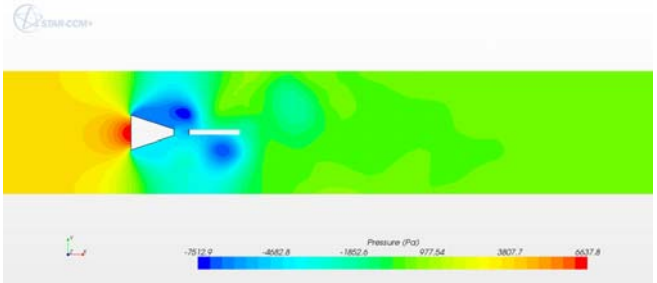

Figure 5: Static pressure for water flow at 2 m/s, undisturbed

The vortices just shed are visible as locations of minimum static pressure. In the initial phase of the present work, the

influence of the single bend on the k-factor at different distances between the bend and the meter were investigated experimentally. However, it was very difficult to interpret the resulting data. It was, therefore, decided to study the effect of the different attributes of the disturbances by comparing following four cases:

a) undisturbed inflow corresponding to a fully developed turbulent profile as given by, for example, Gersten [8]
b) asymmetric inflow only, axial velocity corresponding to Fig. 4 left
c) rotational inflow only, tangential velocity corresponding to Fig. 4 right
d) real single bend inflow obtained from a combination of b) and c)

In all cases, the flow of water in a DN 25 VFM was numerically simulated for a bulk velocity of 2 m/s.

3. NUMERICAL SIMULATIONS

3.1 Undisturbed Inflow

In the case a), the VFM including the pipe of 2.5 D upstream and 5 D downstream was considered. At the inflow boundary, the well known Gersten [8] velocity profile was assumed.

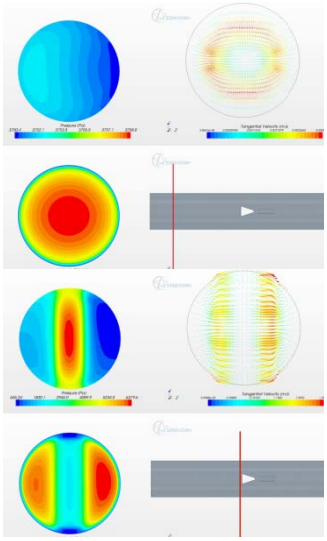

a) b)

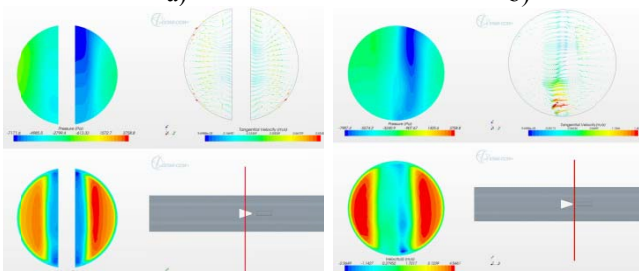

c) d)

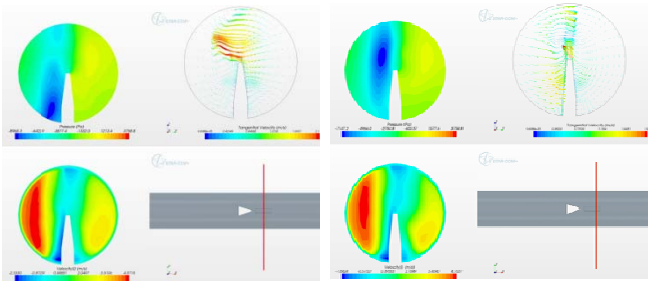

e) f)

Figure 6: Flow field in the VFM with undisturbed inflow; a – f : for location, see corresponding schematic picture

The corresponding axial plane pressure distribution can be seen in Fig. 5. Much more interesting is, however, the flow field development as one proceeds from the bluff body downstream. The series of pictures below is showing the position, the static pressure, the total velocity magnitude and the velocity vectors in the cross-sectional planes. Each of the Figures 6 a) through f) consist of four pictures showing following contours of flow field variables:

Upper left: static pressure
Upper right: vectors of tangential velocity, colored by the total velocity magnitude
Lower left: velocity magnitude
Lower right: schematic view of the axial location

The BB is oriented in vertical direction; for better understanding of the flow features, Figure 5) should be consulted simultaneously. All the Figures 6 a) – f) are facing in negative x-direction , which is in given case upstream.

In Figure 6 a), the flow just after the inflow boundary is shown. Although there seems to be some asymmetry, the relative magnitude of the fluctuations should be considered. It is extremely small. Fig. 6 b) displays the flow just before the BB. The flow field is being split to left and right of the BB. The velocity in the right branch is higher due to the vortex forming downstream of this location. Also visible is the formation of the corner flow between the BB and the pipe wall as dark blue for very low velocity. In Fig. 6 c), the flow situation at the BB is displayed. The distinct asymmetry of the static pressure is caused by the paddle downstream of it. The corner flow with its low velocity and horse-shoe vortex can be seen. The flow in the space between the BB and the paddle, shown in Fig. 6 d), is dominated by the two jets from the space between the BB and the pipe wall, and the wake behind the BB. The tangential velocity at this location is of the same magnitude as the axial velocity, with very significant component from left to right due the vortex flow from the vortex that just separated and is upstream of this location (see Fig.5). The highly non-uniform pressure distribution is already a strong indication of the three-dimensional character of the flow. In Fig. 6 e), the flow over the paddle is displayed. Again, the pressure is dominated by a strong minimum in the left corner with the pipe wall. As the paddle acts as a low aspect ratio wing with high pressure differential, there is a strong tip vortex, in which the tangential speeds are very high. Now, the flow is dominated by the second primary vortex

(below the BB in Fig. 5), resulting in high velocity to the left of the paddle. Further downstream, the axial flow structures develop and change their cross-sectional location, indicating very unsteady flow character. It should be also noticed that due to the shape of the cross-sectional area, the flow in the primary vortices will by no means remain more or less two-dimensional, but will concentrate to a jet-like flow to either side of the vortex. This, again, will induce strong three-dimensional effects.

Finally, the flow downstream of the BB-paddle combination can be seen in Figure 7 a) and b). By comparing this displays with Figures 6, it is obvious that not only is there a significant flow structure lengthwise, but also that these structures are highly unsteady, moving relative to the x-axis. The frequency of these fluctuations is in some cases different but of the same magnitude as the primary vortex shedding frequency, their amplitude potentially larger.

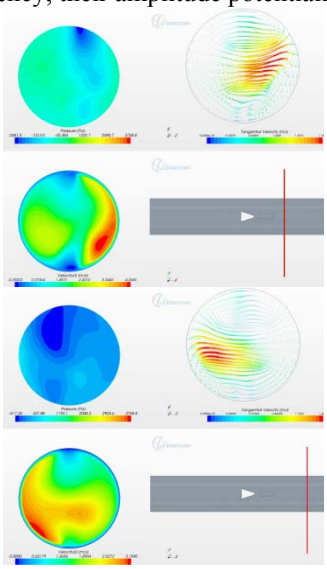

a) b)

Figure 7: Flow field downstream of the VFM

The above discussion is important for understanding the differences between the basic undisturbed flow field in Fig. 6 and 7, and the flow fields with upstream disturbances. In the full paper, the resulting flow of the disturbed inflow cases will be first presented as above, and the differences will be discussed. Finally, the experimental data will be shown and interpreted.

3.2 Single Bend Inflow

After understanding the basic flow field in a VFM, in which the inflow was undisturbed, displaying the typical turbulent velocity profile, the simulation results for a combination of a single bend with the meter section attached to the bend at three different angles of rotation about the x-axis: 0^o, for which the paddle (vortex detection devise) was opposite to the location of the velocity defect in Fig. 4, exposed to the increased axial velocity; 180^o, where the paddle is at the same location as the velocity defect, and 90^o to the plane of the bend will be discussed. The simulation results were summerized in Table 1 below.

feature	**undist.**	**0^o**	**180^o**	**90^o**
F [Hz]	74.67	75.08	72.03	77-79.9
Δf [Hz]	0.0	0.014	0.018	2.9

Table 1: Resulting frequency of vortex shedding as given by flow simulations

In Table 1, f is the main (primary) frequency of vortex shedding. However, in the case of 90^o , the vortex shedding frequencies were different above and below the paddle, called "odd" and "even" frequencies. The difference between these two is shown as Δf. The results for the three orientations of the paddle can be explained as follows:

a) At 0^o, the paddle was behind the area of increased axial velocity, at the "south" wall in Fig. 4. Therefore, the shedding frequency, detected by it, should be higher than for the undisturbed case. Indeed, in this case, the simulated frequency was f = 75.08 Hz, as compared to 74.67 Hz, representing an increase of approximately 0.7 percent.

b) At 180^o, the paddle is exposed the lower incoming velocity and should indicate lower vortex shedding frequency. The simulated result was 3.5 percent lower than in the reference case.

c) At 90^o, the axial velocities were different at the opposite sides of the paddle. This effect lead to a double frequency, one for the higher and one for the lower frequency, called "odd" and "even", being $f_1 = 79.96$ Hz and $f_2 = 77.0$ Hz. The difference between them was $\Delta f = 2.9$ Hz.

Qualitatively, the simulated frequencies agree very well with the expected results and are plausible.

The flow field for the 0^o-case can be seen in Figure 8 at an axial distance from the bend end of 0.8 D.

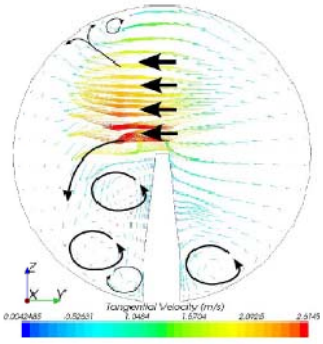

Figure 8: Flow field at the paddle, 0^o-case

In the lower part of the flow field, the two counter-rotating corner vortices can be seen. The primary vortex indeced in this case a significant tangential velocity component from right to left, inducing a vortex in axial direction, similar to induced wing-tip vortices.

The same flow field for the case of 180^o is displayed in Figure 9.

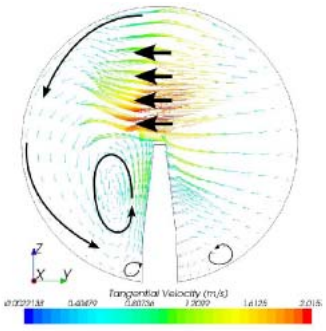

Figure 9: Flow field at the paddle, 180°-case

The corner vortices are in this case somewhat weaker than in Fig. 8, and the primary vortex induces a circumferential velocity seen in the left part of Fig. 9. The maximum tangential velocity located at the end of the paddle, is in this case at v = 2.015 m/s lower than in the case of 0° (v = 2.6 m/s).

The same flow field for the undisturbed case is shown in Fig. 10. Here, the maximum velocity at the paddle is approximately v = 2.12 m/s.

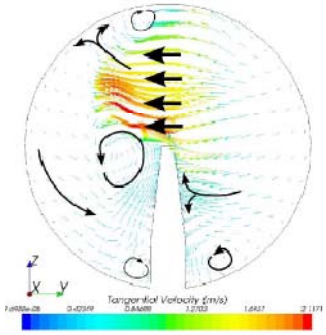

Figure 10: Flow field at the paddle, undisturbed case

4. EXPERIMENTAL RESULTS

In the experimental approach, a commercial vortex-shedding flow meter manufactured by Krohne Messtechnik GmbH was subjected to investigation in the modified testing facility at Krohne Messtechnik GmbH. The fluid being metered was water at pressures up to 5 bar; the measuring section of the meter was DN50.

The test section has been changed to include a simple setup to allow a quick change of the configuration tested. The undisturbed reference case consisted of the basic flow meter with the prescribed upstream and downstream sections of 10 D length of straight pipe. There were the same configurations tested as in the numerical simulations, with different rotations relative between the bend plane and the paddle of the meter. The distance between the bend outlet and the bluff body was also varied, being 0 and 6.4 D. The resulting matrix of possible geometrical configurations included 12 entries. In all cases, the piping could be considered hydraulically smooth. Each configuration was studied at bulk velocities of approximately 0.5, 1.0, 1.5, 3.0 and 5.0 m/s. The corresponding Reynolds numbers Re_D were between 50000 and 250000. The facility included two pumps of different size that were differentially controlled by a CPU using signals from the reference meter (MID). The resulting deviations from the basic reference case without any upstream disturbances were between 0.1 % and almost 2.5 %. The measuring section is shown in Fig. 11.

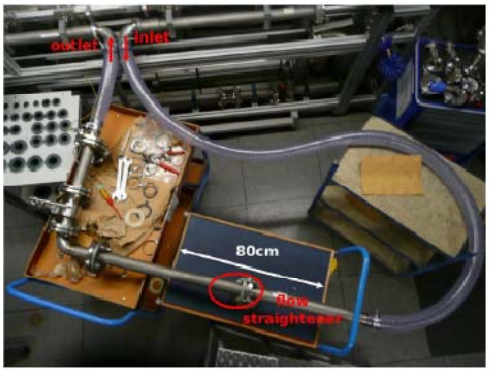

Figure 11: Experimental setup

During the initial stage of the experiments, it became necessary to install a three-plate flow straightener to ensure consistent conditions at the inflow into the bend section. The conditioner can be viewed in Fig. 12.

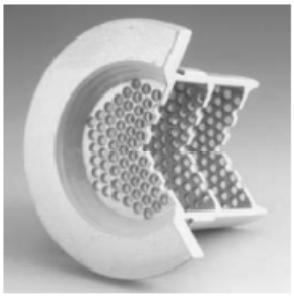

Figure 12: Flow straightener installed in the present work

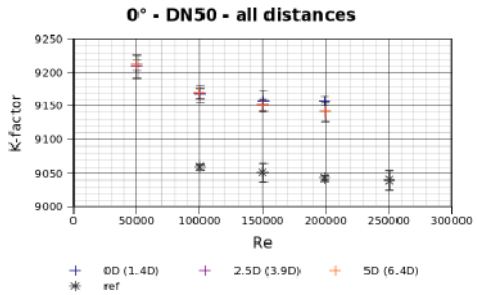

Figure 13 a: K-factor measured for the case of 0° orientation for 4 different distances to the bend

Again, qualitatively, the experimental results agree well with the theoretical considerations as well as numerical simulations. In the case of 0° orientation angle between the paddle and the bend plane, the paddle was exposed to a higher axial velocity and, therefore, displayed higher k-factors than the undisturbed reference case. The difference is, however, somewhat higher than in the simulated data, being approximately 1.6 percent.

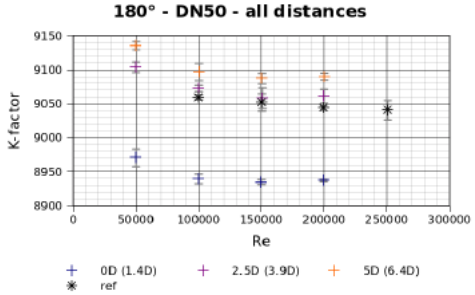

Figure 13 a: K-factor measured for the case of 180° orientation for 4 different distances to the bend

In the case of 180°, with the meter being installed immediately after the bend (0 D), the k-factor is lower than for the reference case, as expected. However, it seems that the effect of non-uniform inflow dissipated relatively quickly, as the k-factors for larger distance from the bend are almost the same as in the reference configuration.

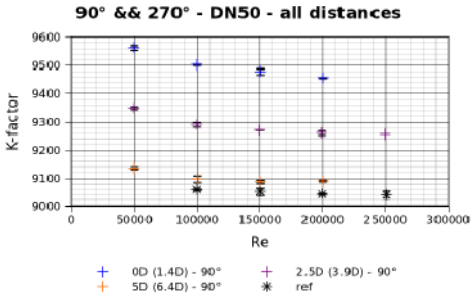

Figure 13 a: K-factor measured for the case of 90° orientation for 4 different distances to the bend

Finally, for the 90° orientation, the measured k-factor is higher than for the reference case, as predicted by the numerical simulation, this effect dissipating again fairly quickly with increasing distance to the bend.

The experimental data was consistent with the numerical simulations, making the explanation of the influence of the bend possible. Presently, the authors are developing a correction method for offsetting the deviation caused by the bend.

5. CONCLUSIONS

The flow fields in typical DN 25 and DN 50 VFM were studied numerically and experimentally. In order to understand the flow field changes due to the disturbances, a detailed investigation of the corresponding flow fields was carried out. Even in the simple case of undisturbed inflow, the flow field was highly complex, displaying an unsteady, three-dimensional character. The bend generated a deviation in the measured and computed k-factors of up to several percent, making correcting measures necessary. The deviation depended in critical way on the relative orientation between the detection paddle and the plane in which the bend was installed. In most cases depending on the orientation, the effect of the bend dissipated relatively quickly. It became very weak when the meter was installed more than approximately 5 D after the bend.

6. REFERENCES

[1] von Lavante, E., Yao, J. and Perpeet, S., „Effects of Disturbed Inflow on Vortex-Shedding from a Bluff Body“, AIAA paper 2000-2220, 2000.

[2] E. von Lavante, U. Banaszak, T. Jubin, S. Tournillon, H. Krisch, „Numerical and Experimental Investigation of Small Size Vortex-Shedding Flow Meter”, Proceedings of the 7th Int. Symposium “Metrologia 2008”, Havana, Cuba, May 2008.

[3] Hans, V., Poppen, G., von Lavante, E., Perpeet, S., “Vortex-shedding flow meters and ultrasound detection: signal processing and bluff body geometry“, Flow Measurement and Instrumentation 9, pp. 79-82, 1998.

[4] Hans, V., Poppen, G., von Lavante, E., Perpeet, S., “Interaction between vortices and ultrasonic waves in vortex- shedding flow meters“, FLUCOME '97, Hayama, 1997.

[5] von Lavante, E., Nath, B. and Färber, J., "Effects of Manufacturing Tolerances on the Accuracy of Vortex-Shedding Flow Meters", XVII IMEKO World Congress on Metrology, Dubrovnik, 2003.

[6] E. von Lavante, U. Banaszak, M. G. Yilmaz, O. Ricken and R. Höcker, ”Effects of Shape Change due to Wear on the Accuracy of Vortex-Shedding Flow Meters”, Proceedings of the 14th Int. Conf. on Flow Measurement Flomeko 2007, Johannesburg, RSA, September 2007.

[7] P. Cambier, S. Vandermarlière, E. von Lavante, U. Banaszak, H. Krisch, S. Tournillon, ”Numerical and Experimental Study of Effects of Upstream Disturbance on Accuracy of Vortex-Shedding Flow Meter”, XIX IMEKO World Congress on Metrology, Lisbon, 2009.

[8] Schlichting, H. and Gersten, K., „Grenzschicht-Theorie“, Springer Verlag, 2006.